https://doi.org/10.5194/egusphere-2023-2155
Preprint. Discussion started: 24 October 2023

Quantifying CH_4 emissions from coal mine aggregation areas in Shanxi, China using TROPOMI observations and the wind-assigned anomaly method

Qiansi Tu[1], Frank Hase[2], Kai Qin[3], Jason Blake Cohen[3], Farahnaz Khosrawi[4], Xinrui Zou[1], Matthias Schneider[1], Fan Lu[3]

[1]Tongji University, School of Mechanical Engineering, Shanghai, China
[2]Karlsruhe Institute of Technology (KIT), Institute of Meteorology and Climate Research (IMK-ASF), Karlsruhe, Germany
[3]China University of Mining and Technology, School of Environment and Spatial Informatics, Xuzhou, China
[4]Forschungszentrum Jülich GmbH, Jülich Supercomputing Centre (JSC), Jülich, Germany

Correspondence to: Qiansi Tu (tuqiansi@tongji.edu.cn), Kai Qin (qinkai@cumt.edu.cn)

Abstract.

China stands out as a major contributor to anthropogenic methane (CH_4) emissions, with coal mine methane (CMM) playing a crucial role. To control and reduce CH_4 emissions, China has made a dedicated commitment and formulated an ambitious mitigation plan. To verify the process made, the consistent acquisition of independent CH_4 emission data is required. This paper aims to implement a wind-assigned anomaly method for the precise determination of regional-scale CMM emissions within the coal-rich Shanxi province. We use the TROPOspheric Monitoring Instrument (TROPOMI) CH_4 observations from May 2018 to May 2023, coupled with ERA5 wind covering the Changzhi, Jincheng and Yangquan regions. The derived emission strengths are $8.4\times 10^{26} \pm 1.6 \times 10^{25}$ molec. s^{-1} (0.706 ± 0.013 Tg yr^{-1}), $1.4 \times 10^{27} \pm 1.9 \times 10^{25}$ molec. s^{-1} (1.176 ± 0.016 Tg yr^{-1}), and $4.9 \times 10^{26} \pm 1.8 \times 10^{25}$ molec. s^{-1} (0.412 ± 0.015 Tg yr^{-1}), respectively. Our results exhibit biases of -18%, 8%, and 14% when compared to the bottom-up inventory. Larger discrepancies are found when comparing the estimates to the CAMS-GLOB-ANT and EDGARv7.0 inventories. This suggests that the two inventories may be overestimating the CH_4 emissions in the Jincheng and Yangquan regions. Our estimates provide a comprehensive characterization of the regions within the Shanxi province, contribute to the validation of emission inventories, and help to develop climate mitigation strategies.

1 Introduction

Methane (CH_4) is the second most important anthropogenic greenhouse gas (GHG) with a relatively shorter lifetime but a larger global warming potential than carbon dioxide (CO_2) (IPCC, 2014; Etminan et al., 2016). For this reason, efforts to reduce CH_4 emission would be beneficial for rapid climate change mitigation in the short term. The atmospheric CH_4 is emitted from a variety of natural sources (accounting for 40%, eg., wetlands, termites) and anthropogenic sources (accounting for 60%, eg. industrial fossil fuel production and consumption, waste disposal, agriculture) (Saunois et al., 2020). Currently, a significant fraction (~33% for the 2008-2017 decade) of global CH_4 emissions related to fossil fuels comes from the exploitation,

https://doi.org/10.5194/egusphere-2023-2155
Preprint. Discussion started: 24 October 2023

transportation, and usage of coal (Saunois et al., 2020). China is one of the leading CH_4 emitters in the world and accounted for around 14-22% of global anthropogenic CH_4 emission (Janssens-Maenhout et al., 2019; Liu et al., 2021; UNFCCC, 2021). In 2021, China pledged to reduce CH_4 emissions under the Glasgow Agreement and intended to develop a comprehensive and ambitious National Action Plan with the goal of achieving a substantial impact on methane emissions control and reductions in the 2020s. Thus, the precise measurement of CH_4 emission changes is essential for determining the effectiveness of these commitments.

The anthropogenic CH_4 emissions in China increased by 40% in the 2000s (Liu et al., 2021), probably reflecting increasing coal production (Gao et al., 2021). Coal production in China reached 3.9 Gt in 2020, with approximately half of the coal being utilized for thermal power generation (National Bureau of Statistics of China, 2022). China's official GHG emission inventory (MEE, 2019) reports that the country's coal mine methane (CMM) emissions amounted to about 21 Tg in 2014, thus accounting for 38% of its total anthropogenic CH_4 emissions. China has submitted three versions of the National Communications on Climate Change (NDRC, 2004, 2012; MEE, 2019b) and two reports of Biennial Update Reports on Climate Change since 2004 (NDRC, 2017; MEE 2019a), in which the estimated inventories of the CMM emissions are reported. The current CMM emission inventories are usually based on bottom-up data-based approaches, which involves identifying and quantifying the CH_4 emissions from each type of coal mine (Gao et al., 2020).

Mainland China's coal mines are spread across 26 provinces and were comprised of approximately 1000 coalfields and over 10,000 coal mines in 2011 (SACMS, 2012). The CMM emissions in China show unique characteristics and complexities, due to the large variability of the coal rank, capacity, geological conditions, and mining technologies of the numerous coal mines (Gao et al., 2020, 2021; Peng et al., 2016; Scarpelli et al., 2020). This large number of coal mines and the heterogeneity between them also induce considerable uncertainties in bottom-up estimates and so are a challenge in achieving accurate CMM emissions (Sheng et al., 2019). Therefore, a strong demand exists for independent and objective verification of CMM emissions from local to regional scales based on atmospheric observations, which are commonly known as top-down approaches. The observations from satellite, e.g. the TROPOspheric Monitoring Instrument (TROPOMI) on board the Sentinel-5 Precursor satellite, provide the ability to estimate the CMM emissions on both global and regional scales (Sadavarte et al., 2021; Tu et al., 2022b).

This study conducts the wind-assigned anomaly method (Tu et al., 2022a, b) on TROPOMI XCH_4 observations from 2018 to 2023 over three subregions in Shanxi province to determine the CMM emissions over that period. Shanxi province is known for its abundant coal reserves and is considered one of the coal-richest provinces in China. The coal production in Shanxi exceeded 1 billion tons in 2021, accounting for nearly one-third of the country's total coal output and 12% of the global output. This highlights the significant role of Shanxi province in China's energy sector and emphasizes the importance of estimating CMM emissions from the mining activities in the region. In this work, the emission estimation method and the TROPOMI dataset are introduced in Sect. 2. In Sect. 3 we present the results of the TROPOMI observations and three different inventories

https://doi.org/10.5194/egusphere-2023-2155
Preprint. Discussion started: 24 October 2023

used for comparison, followed by estimated CMM emissions over three subregions. An uncertainty analysis based on a dispersion model, wind information and inventory is also performed in this section. A conclusion is given in Sect. 4.

2 Data and method

2.1 TROPOMI dataset

Launched in October 2017, the TROPOMI instrument is an imaging spectrometer which is designed to view the Earth in nadir direction. The instrument utilizes passive remote-sensing techniques to measure solar radiation reflected by and radiated from the Earth across the ultraviolet (UV), visible (VIS), near-infrared (NIR), and short-wave spectral (SWIR) bands (Veefkind et al., 2012). The instrument is capable of providing an unprecedented high spatial resolution (5.5 × 7 km^2) and complete daily global coverage of the CH_4 total column-averaged dry-air mole fraction (XCH_4) (Veefkind et al., 2012; Lorente et al., 2021). The RemoTec algorithm, which has been widely utilized in deriving CH_4 and CO_2 from the Greenhouse Gases Observing Satellite (GOSAT) (Butz et al., 2009, 2011; Guerlet et al., 2013), is also deployed here to retrieve XCH_4 from TROPOMI measurements. These measurements capture sunlight backscattered by the Earth's surface and atmosphere in the NIR and SWIR spectral bands (Hu et al., 2018). Recent studies show the potential of using high-resolution TROPOMI XCH_4 for detection and quantification of the CH_4 emissions. TROPOMI observations have been used for quantifying CH_4 emissions from the oil and gas sector (Pandey et al., 2019; Varon et al., 2019; de Gouw et al., 2020; Schneising et al., 2020; Zhang et al., 2020), from urban areas (Tu et al., 2022a; Foy et al., 2023; Plant et al., 2022), and from coal mining (Sadavarte et al., 2021; Tu et al., 2022b). In this study, the TROPOMI XCH_4 observations spanning the period from May 2018 to May 2023 over the study areas in the Shanxi province are used.

2.2 Wind-assigned anomaly method

The wind-assigned anomaly method was first developed in quantifying CH_4 emissions from landfills in Madrid (Tu et al., 2022a). Its applicability for estimating the CMM emissions in the Upper Silesian Coal Basin (USCB) in southern Poland was demonstrated afterwards (Tu et al., 2022b).

The CH_4 emerging from a point source is expected to be distributed along the wind direction. It is assumed that the CH_4 molecules disperse evenly along a fan-shaped plume (Tu et al., 2022a Fig 2). The column enhancement in the downwind side due to the assumed source is represented by the following equation:

$$dcol_{CH_4} = \frac{\varepsilon}{v \cdot d \cdot fov} \quad \textbf{Eq. (1)}$$

wherein ε represents the emission rate at the source point in molec. s^{-1}, v is the wind speed in ms^{-1}, d the distance between the source point and the downwind point, and fov the opening angle of the cone plume in rad. Here fov is assumed to be 60° based on previous studies (Tu et al., 2022a, b). It should be noted that the point source does not generate enhanced CH_4 concentrations outside of the cone. This may introduce some uncertainties and will be discussed in Sect. 3.4.

https://doi.org/10.5194/egusphere-2023-2155
Preprint. Discussion started: 24 October 2023

3. Results and discussion

3.1 TROPOMI observations

Shanxi province is rich in coal resources, and as a result, there are more than 600 coal mines spread across the province. Most of these coal mines are concentrated in the northern, eastern and southeastern, and central regions of China. A multi-year average of TROPOMI XCH_4 observations in the whole Shanxi province is shown in Figure 1, superimposed to the locations of mines in the area. Elevated XCH_4 is observed in three regions: Yangquan (east), Changzhi (southeast) and Jincheng (south). Of these regions, the Changzhi region is of particular interest since a field campaign was implemented in 2022. This field campaign region covers an area of 35.8ºN–37.2ºN, 112.6ºE–113.6ºE, i.e., 155 km × 90 km) and will be discussed in detail as an example to better understand the CH_4 emissions from coal mining activities in Shanxi province.

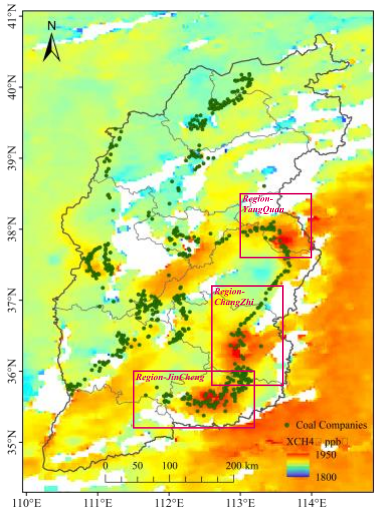

Figure 1: TROPOMI XCH_4 and the location of coal mines in Shanxi province. Dot symbols denote the coal mine locations (http://nyj.shanxi.gov.cn/, last access: August 21, 2023).

There are 62 coal mines located over the study area in Changzhi region, as shown in Figure 2. The emission rates range from 1.6×10^{24} to 1.4×10^{26} molec. s^{-1} (~0.001 Tg yr^{-1} – 0.11 Tg yr^{-1}) (Qin et al., 2023). Near 30 small coal mines scatter in the mountain area in the south and the emissions are relatively small with 24 orders of magnitude in molec. s^{-1}. Some larger coal mines with higher emissions rates (emission rate > 1.0×10^{25} molec. s^{-1}) are close to the Zhangzi county as well as in the north region and the mean value is around 7.3×10^{25} molec. s^{-1} with a standard deviation of 4.6×10^{25} molec. s^{-1}.

https://doi.org/10.5194/egusphere-2023-2155
Preprint. Discussion started: 24 October 2023

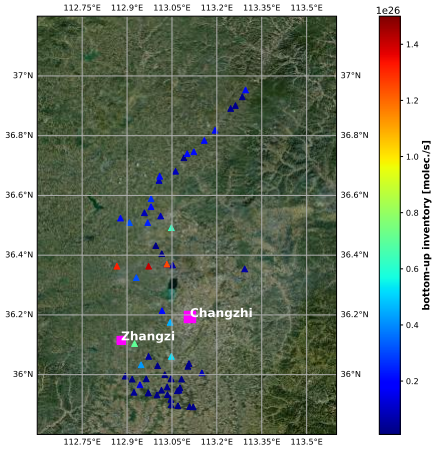

Figure 2: Terrain map with bottom-up inventory (Qin et al., 2023). The triangle symbols represent the location of all individual coal mines, and different colors denote the emission rates. The square symbols denote the locations of Changzhi city and Zhangzi county. Terrain information originates from World Imagery.

A time series of five-years of TROPOMI XCH_4 observations in the Changzhi region is shown in Figure 3. The average concentration is 1906.8 ± 41.0 ppb over the entire period. From 2019 to 2022, there is an observed increase in XCH_4 levels by approximately 0.7% per year. The observations in the figure indicate that there is a clear seasonal variability in the concentrations. The data shows that the lowest abundances of XCH_4 occur in the early part of the year, while the highest values are observed in autumn. The seasonal pattern is determined by both sinks and sources. The elimination of methane (CH_4) by hydroxyl radicals (OH) in the troposphere, known as atmospheric oxidation, plays a crucial role in controlling the concentrations of climate-relevant gases like CH_4 (Rigby et al., 2017; Li et al., 2018). This process is responsible for approximately 85-90% of atmospheric CH_4 loss (Saunois et al., 2020). On the other hand, the dominant factor contributing to CH_4 emissions in this region is coal mining activities. These coal production activities can vary throughout the year and have a significant impact on the overall XCH_4 concentrations.

https://doi.org/10.5194/egusphere-2023-2155
Preprint. Discussion started: 24 October 2023

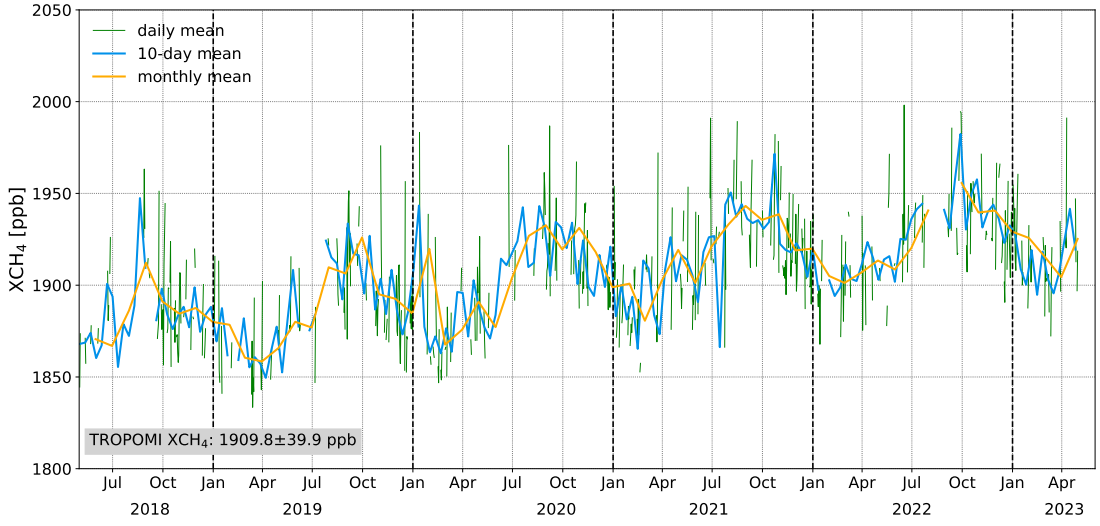

Figure 3: Time-series of average TROPOMI XCH_4 over Changzhi region (35.8ºN—37.2ºN, 112.6ºE—113.6ºE) from May 2018 to April 2023.

3.2 CH_4 inventories

CAMS Global anthropogenic emissions (CAMS-GLOB-ANT) inventory provides methane emissions for different sectors with a spatial resolution of 0.1º × 0.1º and temporal coverage from 2000 to 2024 (Granier et al., 2019; https://permalink.aeris-data.fr/CAMS-GLOB-ANT, last access: 12 July 2023). Emissions are provided as monthly and yearly averages and v5.3, which includes updated ship emissions from CAMS-GLOB-SHIP v3.1, is used in this study. The yearly mean of CAMS-GLOB-ANT for 14 sectors are illustrated in Figure 4a. Emissions from maritime transport in the study area are zero and not shown here. The inventory very well presents the dominant emission sources in the study area. The coal production (fugitives (coal)) is the dominant source of methane emissions, accounting for ~96% in total emissions. The sector of solid waste and waste water is the secondary emission source which drops to 2%. Figure 4b shows the spatial distribution of coal emission. The locations of the coal mines and the corresponding emission rates fit well with the CAMS inventory. About half of the coal mines are concentrated in the southern region, while the other half are located further north, along a southwest to northeast direction. The two reddish grids (36.05ºN-36.15ºN, 113.05ºE) denote the highest emission rate in the CAMS inventory, partly due to the Changzhi city, which is located nearby. The CH_4 emission in the city region are primarily attributed to the traffic (particularly during the morning and evening rush hours), CH_4 leaks at gas stations and the utilization and release of natural gas in residential areas (Liu et al., 2022). The CH_4 emission accounts for 1.77×10^{27} molec. s^{-1} (1.5 Tg yr^{-1}) for the whole study area, which is 55% higher than the bottom-up inventory (1.14×10^{27} molec. s^{-1} ~ 0.96 Tg yr^{-1}).

https://doi.org/10.5194/egusphere-2023-2155
Preprint. Discussion started: 24 October 2023

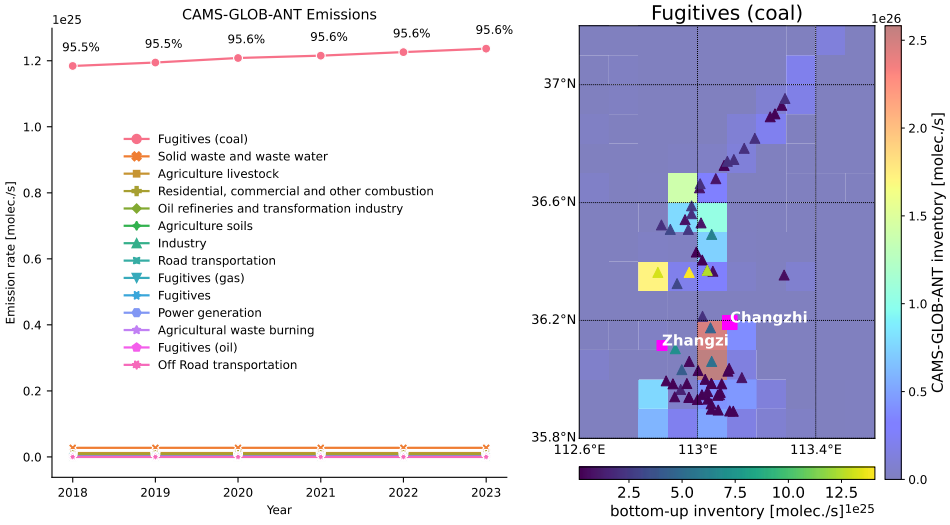

Figure 4: Left: time-series plot of the yearly averaged CAMS global anthropogenic emissions for different sectors for 2018–2023 (https://permalink.aeris-data.fr/CAMS-GLOB-ANT, last access: 12 July 2023, Granier et al., 2019). The percentage values represent the share of methane emission from coal production and distribution (fugitives (coal)). Right: spatial distribution of methane emission from coal production for the CAMS-GLOB-ANT inventory. The triangle symbols denote the locations of the coal mines and the respective colors represent their emission rates based on the bottom-up inventory (Qin et al., 2023).

The latest EDGARv7.0 emission inventory is the first product of the new Emissions Database for Global Atmospheric Research (EDGAR) Community GHG emissions database (Crippa et al., 2021), which provides estimates of emissions of the three main GHGs (CO_2, CH_4 and N_2O) and fluorinated gases per sector and country. The dataset offers the same spatial resolution of 0.1° × 0.1° as the CAMS inventory and covers the period of 1970 to 2022. The CH_4 emissions from the fuel exploitation sector are the dominant sources in the study area, which accounts for 95.5% from 2018-2021. The total estimates originating from the energy sector are around 1.85×10^{27} molec. s^{-1} (1.6 Tg yr^{-1}). The EDGARv7 estimates present a very similar spatial distribution (Figure A- 1) as the CAMS inventory with slightly higher (4.5%) values.

3.3 Estimation of CH_4 emission strengths from TROPOMI data sets

The ERA5 wind at 100 m altitude above ground is used for describing the transport for the wind-assigned method. The wind is segmented as NW (>215° and <45°) and SE (45° – 215°) fields for Changzhi region (Figure A- 2). Due to the observed seasonal changes in XCH_4, the observed variable background concentrations need to be considered when estimating the emissions. The TROPOMI enhancements after removing the background are shown in Figure 5a. High values are observed in the center and south of the study area, i.e., close to the clusters of the coal mines (triangle symbols). It is difficult to distinguish the CH_4 from the residential regions since the coal mines are located close to Zhangzi county and Changzhi city. The averaged enhancements are 4.7 ppb ± 5.6 ppb for the whole region. The wind-assigned anomalies from the TROPOMI observations indicate the difference of the enhancements for wind coming from NW and from SE, resulting in a positive plume in the SE direction and negative plume in NW direction (Figure 5b).

https://doi.org/10.5194/egusphere-2023-2155
Preprint. Discussion started: 24 October 2023

The correlation of the wind-assigned anomalies deduced from the TROPOMI observations and from the plume model using the bottom-up inventory is presented in Figure 5c, and the estimated emission rate is $8.4 \times 10^{26} \pm 1.6 \times 10^{25}$ molec. s^{-1} (R^2 = 0.61). The bottom-up, CAMS and EDGARv7 inventories are overestimated, with 31%, 120% and 130% higher than the estimate based on the TROPOMI observations and the wind-assigned method, respectively.

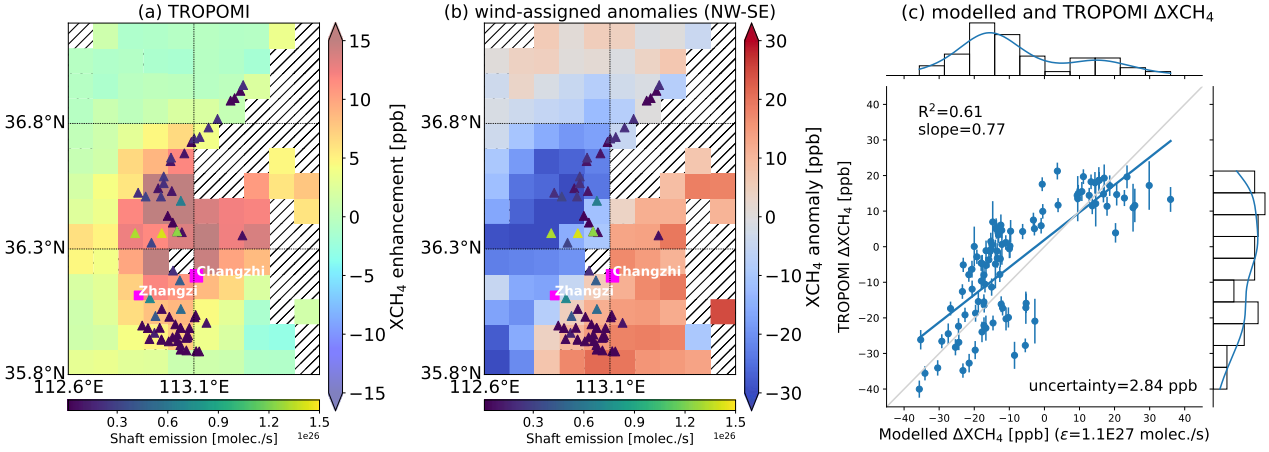

Figure 5: TROPOMI XCH_4 enhancement (XCH_4-background) (a), the wind-assigned anomalies (NW–SE) (b), and correlation plot of the wind-assigned anomalies (c) between TROPOMI and the simple cone plume model with using the bottom-up inventory (1.1×10^{27} molec. s^{-1} in total) and ERA5 wind at 100 m during May 2018–May 2023 over the Changzhi region. The triangle symbols denote the inventory locations, with different colours indicating varying emission rates. Hatched areas in (a)–(b) indicate grids with no available data. The uncertainty in (c) is presented by the average error bars of the anomalies, which are derived from the uncertainty in the background and the TROPOMI observations.

The wind-assigned method was also applied to Jincheng and Yangquan regions. The wind segmentations are NW-SE for Jincheng and E-W for Yangquan based on the ERA5 wind information (Figure A- 2). The estimated emission is $1.4 \times 10^{27} \pm 1.9 \times 10^{25}$ molec. s^{-1} for Jincheng and $4.9 \times 10^{26} \pm 1.8 \times 10^{25}$ molec. s^{-1} for Yangquan. The wind-assigned anomalies in the Jincheng region shows a better correlation with a R^2 value of 0.80, whereas the value is lower (R^2=0.42) in the Yangquan region (Figure A- 6). The resulting estimate for Jincheng is close to the bottom-up inventory, displaying a minor deviation of around 8%. However, the distinction is more pronounced for Yangquan, exhibiting a slightly larger difference of 14%. Figure 6 summarizes the estimated emissions based on the wind-assigned anomaly method compared to the predictions based on the inventories in all regions. In general, the estimates are comparable to the bottom-up inventory, whereas both CAMS and EDGAR inventories overestimate the emissions with a relative difference of about 120%/130% in Changzhi, 60%/68% in Jincheng and 165%/186% in Yangquan.

https://doi.org/10.5194/egusphere-2023-2155
Preprint. Discussion started: 24 October 2023

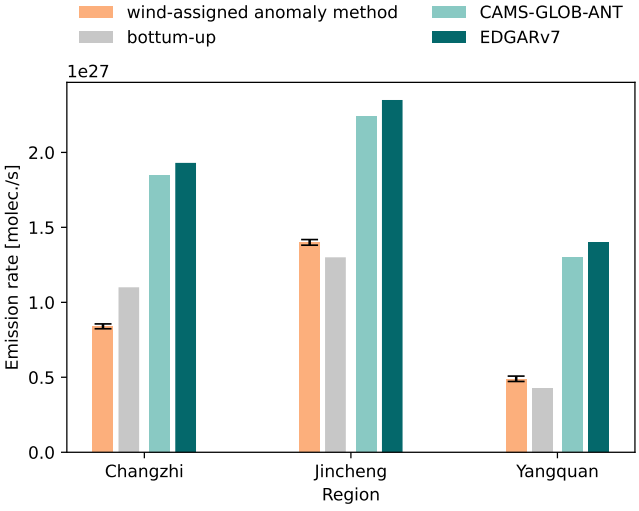

Figure 6: Estimated emission rates and emission rates from three different inventories for the Changzhi, Jincheng and Yangquan regions.

3.4 Uncertainty analysis

3.4.1 Cone plume and Gaussian plume model

The wind-assigned method uses the cone plume model, in which the emitted molecules are dispersed evenly within a cone-shape area (Tu et al., 2022a, b). To evaluate the sensitivity of the analysis with respect to the assumption, an alternative Gaussian plume is investigated in the following.

$$dcol_{CH_4} = \frac{\varepsilon}{v \cdot d \cdot \sqrt{2\pi} \cdot (\frac{\text{fov}}{2})} \cdot \exp\left(-\frac{1}{2} \cdot (\frac{\varphi}{(\frac{\text{fov}}{2})})^2\right) \quad \textbf{Eq. (2)}$$

where $dcol_{CH_4}$ represents the enhanced column in the downwind direction, the fov the angle of the opening angle adopted from the cone plume model (Tu et al., 2022a), v the wind direction, d the distance between the point source and the downwind location, and φ the angle of plume axis and the direction under consideration. The $dcol_{CH_4}$ in the cone plume is restricted in the cone area with an opening angle of fov, while the values in the Gaussian plume show a gradually fading enhancement along the circle arc at any radius d (Figure A- 8).

To further investigate the uncertainty of the two plume models, different opening angles are tested for estimating CH_4 emissions in the Changzhi region. Estimated emissions increased with increasing fov for both plume models. The results based on the Gaussian plume is higher than those based on the cone plume and the discrepancy between the two models increases with increasing opening angle. When the fov is chosen as the previous setting value (60°), the estimated emission rate based on the Gaussian plume are $9.4 \times 10^{26} \pm 1.7 \times 10^{25}$ molec. s^{-1}, which is 12% higher that based on the cone plume model. The relative difference between these two models drops to 5% for fov = 20°. The anomalies derived from the Gaussian plume

https://doi.org/10.5194/egusphere-2023-2155
Preprint. Discussion started: 24 October 2023

model is overall similar to those from the cone plume model, showing a slightly better correlation with the anomalies from the TROPOMI observations (R^2 = 0.65, Figure A- 9).

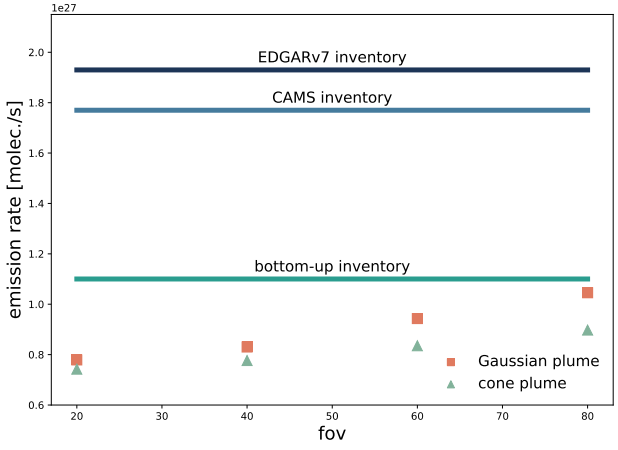

Figure 7: Estimates of emission rates in Changzhi region with respect to different opening angles based on cone plume and Gaussian plume. The three different inventories are presented as well.

3.4.2 Wind analysis data and field segmentation

Uncertainty in wind direction and speed is one of the largest sources of error in correctly estimating the emission rates (Tu et al., 2022b). Thus, another wind dataset and the wind field segmentation associated with the wind-assigned method are investigated.

An alternative wind dataset at a height of 100m above the ground from the Global Data Assimilation System (GDAS) are used instead of the ERA5 dataset. The GDAS provides the National Centers for Environmental Prediction (NCEP) FNL (Final) operational global analysis and forecast data with a spatial resolution of 0.25° × 0.25° and a temporal resolution of 6 h (National Centers for Environmental Prediction et al., 2015). Compared with the ERA5 data, the NCEP data shows comparable wind distributions (Figure A- 7), featuring slightly elevated wind speeds and a more prevalent wind direction originating from the broader northwest region. The estimated emission strength for using the NCEP dataset amounts to $7.9 \times 10^{26} \pm 1.6 \times 10^{25}$ molec. s^{-1}, indicating a reduction of 5% compared to the value obtained when using the ERA5 dataset. The wind segmentation is mainly based on the local predominant wind. To quantify its uncertainty, different division (N and S segmentations) is applied. The CH_4 emission is slightly higher (12%) than that using NW-SE wind segmentation with an approximate value of $9.2 \times 10^{26} \pm 1.8 \times 10^{25}$ molec. s^{-1}.

3.4.3 Inventories

The use of an inventory as a priori knowledge is integral to the wind-assigned anomaly approach. As detailed in Sect. 3.2, the bottom-up and the CAMS-GLOB-ANT (or EDGAR) inventories highlight discrepancies in emission sources both in terms of location and abundance. To investigate the uncertainty introduced by the inventory, the CAMS-GLOB-ANT inventory is

https://doi.org/10.5194/egusphere-2023-2155
Preprint. Discussion started: 24 October 2023

employed in the approach instead of the bottom-up inventory. Given the similarity in pattern between the CAMS and EDGAR inventories, we have exclusively focused on the CAMS inventory. This substitution leads to minor deviations in the enhancements (XCH_4 - background) observed across the Changzhi region (Figure A- 10a). In general, the spatial patterns maintain a notable similarity, while presenting some divergence in abundance. The calculated average stands at 3.61 ± 4.44 ppb when employing the CAMS-GLOB-ANT inventory. In contrast, using the bottom-up inventory yields an average of 4.68 ± 5.59 ppb. The wind-assigned anomalies from both datasets also present comparable patterns and display a strong correlation between them (Figure A- 10b, R^2 = 0.9962). It is because the systematic errors in background removal is compensated by computing the differences of enhancements under different wind field segmentations. The estimated emission strength amounts to $8.5 \times 10^{27} \pm 1.8 \times 10^{25}$ molec. s^{-1}. Replacing the bottom-up inventory with the CAMS-GLOB-ANT inventory introduces a minor bias.

4. Conclusion

Quantifying CMM emissions using high-spatial resolution satellite observations can contribute independent emission estimates for evaluating inventories and assisting in the development of reduction strategies and interventions. In this study, a wind-assigned anomaly method was used for analyzing the TROPOMI XCH_4 observations between May 2018 to May 2023. The CMM emissions in three subregions (Changzhi, Jincheng, Yangquan) in the coal-rich Shanxi province of China were achived. The three regions are aggregation areas of coal mines, consequently exhibiting elevated XCH_4 abundances. The concluded emission strengths are $8.4\times 10^{26} \pm 1.6 \times 10^{25}$ molec. s^{-1} (0.706 ± 0.013 Tg yr^{-1}), $1.4 \times 10^{27} \pm 1.9 \times 10^{25}$ molec. s^{-1} (1.176 ± 0.016 Tg yr^{-1}), and $4.9 \times 10^{26} \pm 1.8 \times 10^{25}$ molec. s^{-1} (0.412 ± 0.015 Tg yr^{-1}), respectively.

When comparing the estimates with three different inventories (bottom-up, CAMS-GLOB-ANT, and EDGARv7.0), the estimates obtained using the wind-assigned anomaly method are comparable to the bottom-up inventories, with relative differences of 31%, -7%, and -12% in Changzhi, Jincheng, and Yangquan, respectively. The CAMS-GLOB-ANT and EDGARv7.0 inventories show very similar results. However, higher discrepancies are found when comparing our estimates to these inventories, with differences reaching approximately 125%, 64%, and 176%, respectively. This suggests that the CAMS-GLOB-ANT and EDGARv7.0 inventories might overestimate the CH_4 emissions from these coal mining regions.

The cone plume model introduces uncertainties due to assuming a sharply boarded fan-shaped plume extending along the downwind direction, i.e., any points located outside of the cone area experience no enhancement. To estimate the uncertainties connected to the assumed plume shape, we investigate the assumption of a Gaussian plume, resulting in an estimated emission strength increase of 12%. Beyond the consideration of the dispersion model, the assumed wind speed and direction is a major source of uncertainty. We analyze the impacts of using another wind dataset (NCEP FNL) for the analysis, revealing a minor bias of -5%. Additionally, we tested an alternative wind category (N-S), yielding a 12% increase in estimated emission strength. The emission inventory is considered as a priori knowledge in the approach and replacing the bottom-up inventory with the CAMS-GLOB-ANT inventory introduces a very small bias of (1%).

https://doi.org/10.5194/egusphere-2023-2155
Preprint. Discussion started: 24 October 2023

This study further demonstrates the practicality of employing the wind-assigned anomaly method together with the high spatial resolution TROPOMI XCH_4 to quantify regional-scale CH_4 emission strengths. This approach holds promise for extending its application to estimate CMM emission in other coal mine-active regions, thereby providing top-down estimates that can enhance the refinement of inventories. Moreover, these results offer support for enhancement of the mitigation strategies and the efficient control of CMM emissions.

Data availability. The TROPOMI data set is publicly available from https://scihub.copernicus.eu/ (last access: 29 July 2023; ESA, 2020). The access and use of any Copernicus Sentinel data available through the Copernicus Open Access Hub are governed by the legal notice on the use of Copernicus Sentinel Data and Service Information, which is given here: https://sentinels.copernicus.eu/documents/247904/690755/Sentinel_Data_Legal_Notice (last access: 29 July 2023; European Commission, 2020).

Author contributions. QT and FH developed the research question. QT wrote the manuscript and performed the data analysis with input from FH. QK supplied the bottom-up inventory and local insights for the study regions. XZ designed and created parts of the graphics. FK and QK participated in result discussions and contributed to improve the paper. All authors contributed to the interpretation of the results and the improvement of the manuscript.

Competing interests. At least one of the (co-)authors is a member of the editorial board of Atmospheric Chemistry and Physics.

Acknowledgements. We would like to thank Emissions of atmospheric Compounds and Compilation of Ancillary Data (ECCAD) for providing CAMS-GLOB-ANT inventory data and the Emissions Database for Global Atmospheric Research (EDGAR) for providing EDGARv7.0 inventory data. Thanks should also go to the TROPOMI team for making CH_4 data publicly available.

Financial support. This study was supported by the National Natural Science Foundation of China (grant no. 42305138) and the Shanxi Province Major Science and Technique Program (grant no. 202101090301013).

https://doi.org/10.5194/egusphere-2023-2155
Preprint. Discussion started: 24 October 2023

Appendix

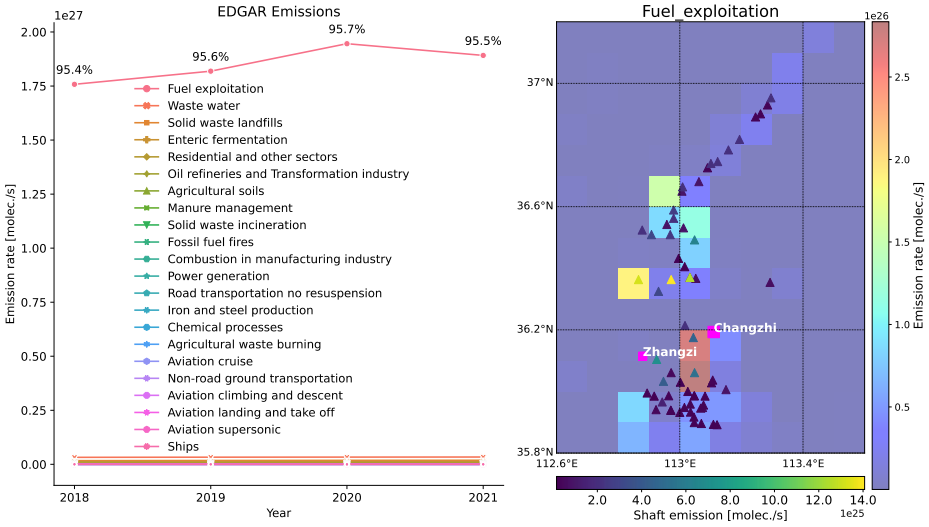

Figure A- 1: Similar to Figure 4 but for the EDGARv7 energy sector.

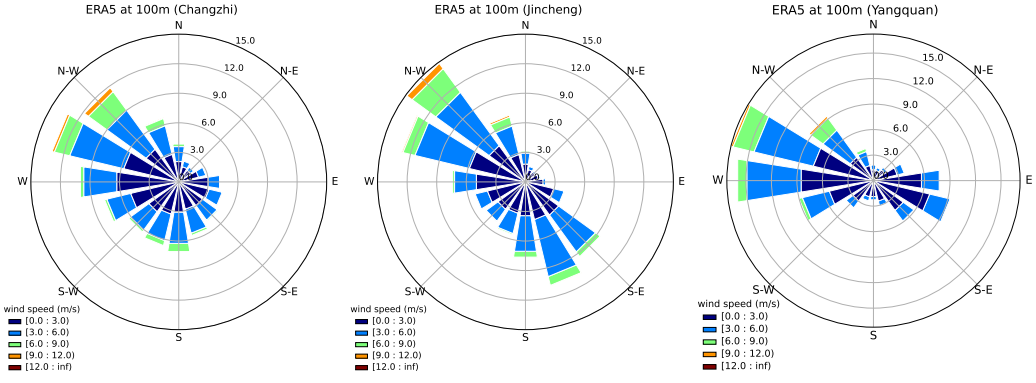

Figure A- 2: Wind roses plots for local daytime (08:00–18:00 UTC) from May 2018 to April 2023 for the ERA5 model wind in Changzhi, Jincheng and Yangquan regions, respectively.

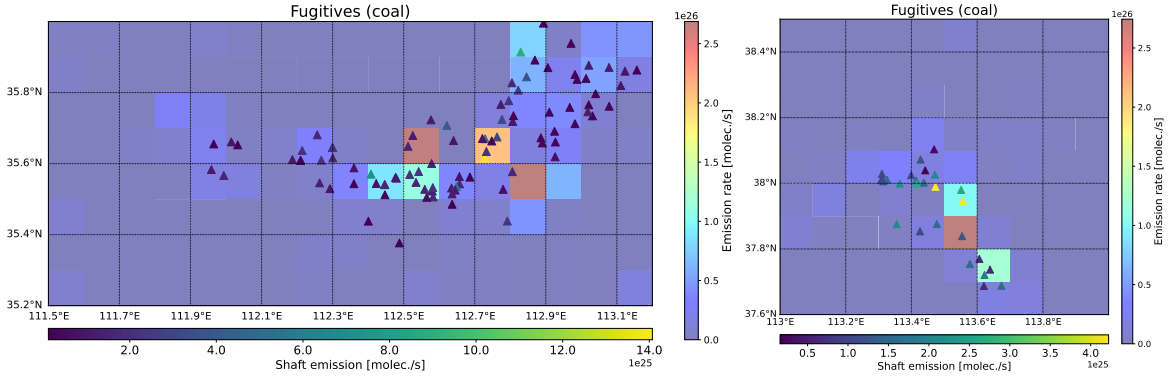

https://doi.org/10.5194/egusphere-2023-2155
Preprint. Discussion started: 24 October 2023

Figure A- 3: Similar to Figure 4-right, but for Jincheng (left) and Yangquan (right) regions, respectively.

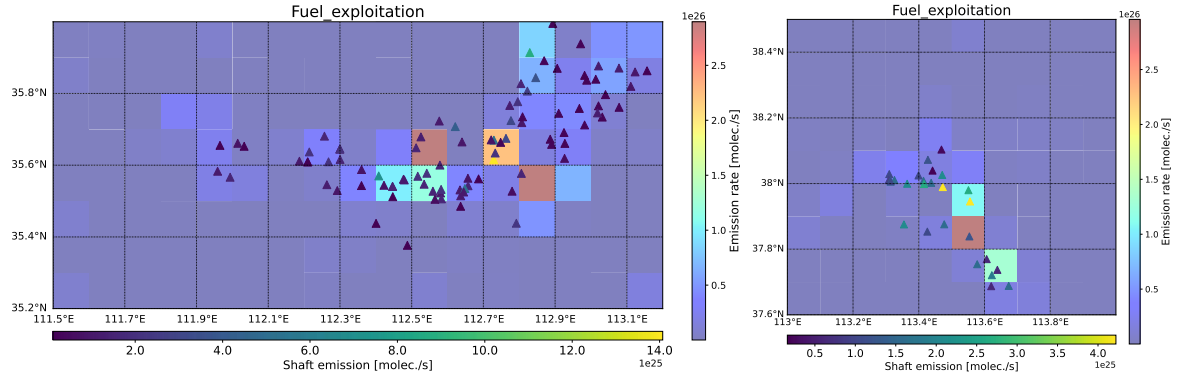

Figure A- 4: Similar to Figure 4-right, but for the EDGARv7 energy sector in Jincheng (left) and Yangquan (right) regions, respectively.

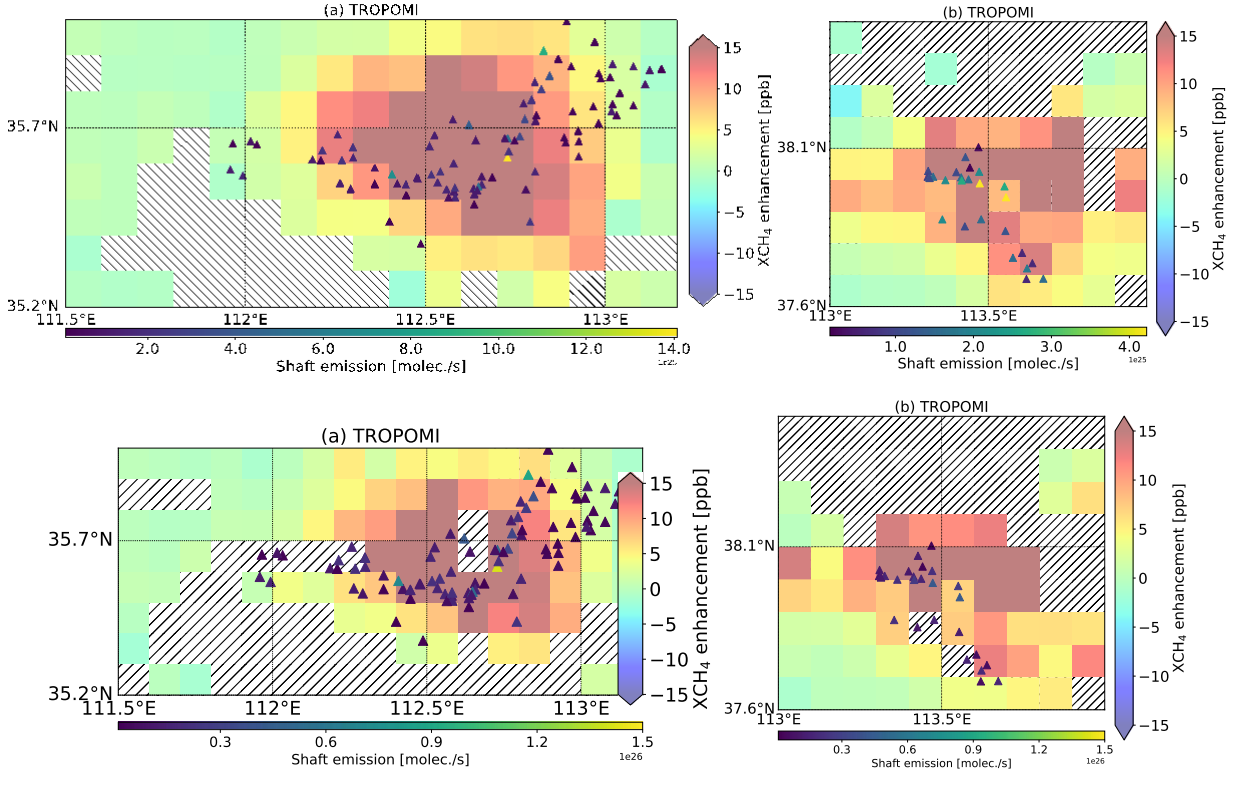

Figure A- 5: XCH_4 enhancements (XCH_4 - background) for Jincheng and Yangquan region.

https://doi.org/10.5194/egusphere-2023-2155
Preprint. Discussion started: 24 October 2023

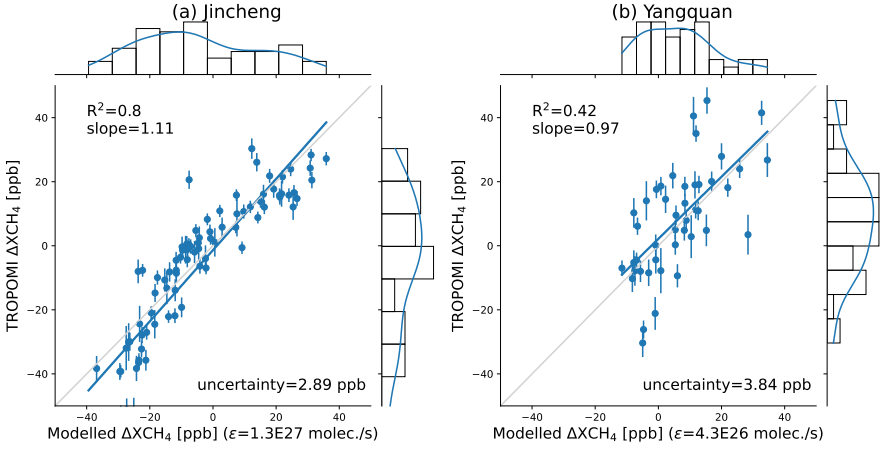

Figure A- 6: Similar to Figure 5(c), but for the Jincheng and Yangquan regions.

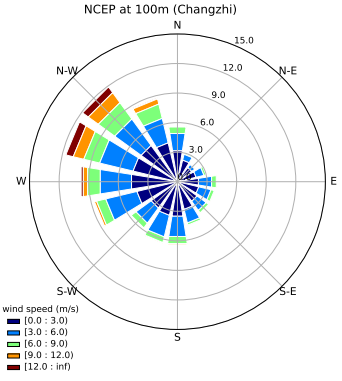

Figure A- 7: Similar to Figure A- 2(a) but from NCEP FNL operational analysis data in the Changzhi region.

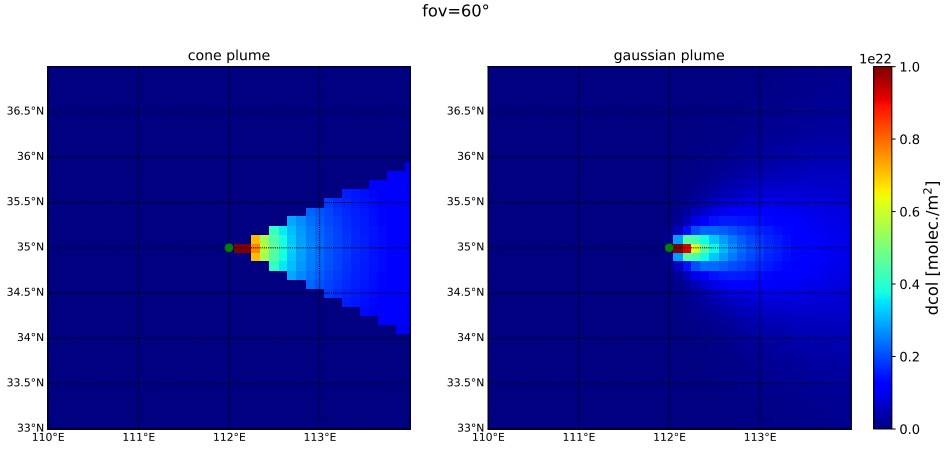

Figure A- 8: spatial distribution of dispersion based on the cone plume and Gaussian plume model. The wind from west is used as an example.

https://doi.org/10.5194/egusphere-2023-2155
Preprint. Discussion started: 24 October 2023

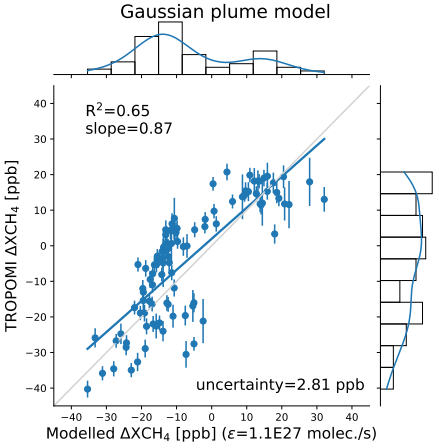

Figure A- 9: Similar to Figure 5(c) but using the Gaussian plume model.

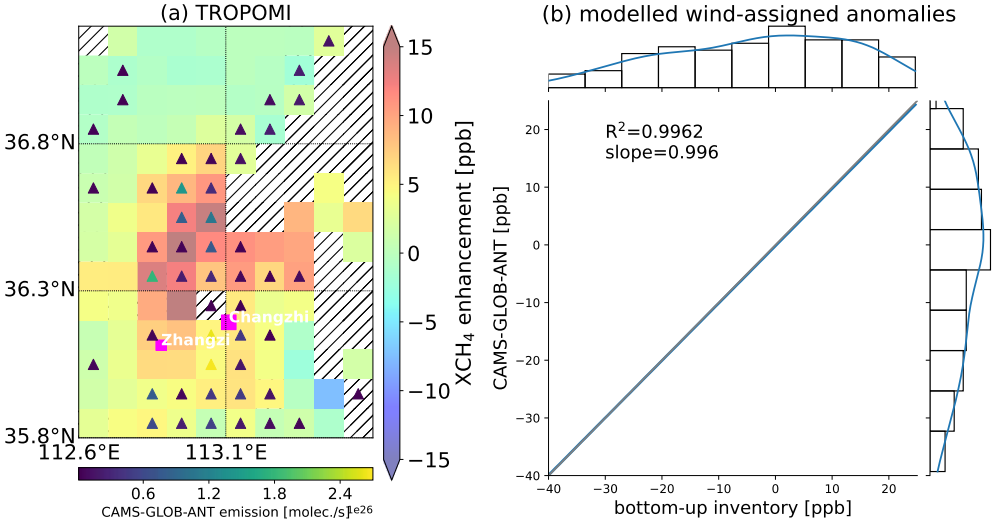

Figure A- 10: (a): similar to Figure 5(a) but using the CAMS-GLOB-ANT inventory as the a prior information. The triangle symbols denote the inventory location (emission rate > 1 × 10^{24} molec. s^{-1}). (b): correlation between using the bottom-up inventory and the CAMS-GLOB-ANT inventories for the modelled wind-assigned anomalies.

References

Butz, A., Hasekamp, O. P., Frankenberg, C., and Aben, I.: Retrievals of atmospheric CO2 from simulated space-borne measurements of backscattered near-infrared sunlight: accounting for aerosol effects, Appl. Opt., 48, 3322–3336, 2009.

Climate Change 2014: IPCC: Synthesis Report. Contribution of Working Groups I, II and III to the Fifth Assessment Report of the Intergovernmental Panel on Climate Change, edited by: Core Writing Team, Pachauri, R. K., and Meyer, L. A., IPCC, Geneva, Switzerland, 151 pp., 2014.

https://doi.org/10.5194/egusphere-2023-2155
Preprint. Discussion started: 24 October 2023

Crippa, M., Guizzardi, D., Solazzo, E., Muntean, M., Schaaf, E., Monforti-Ferrario, F., Banja, M., Olivier, J.G.J., Grassi, G., Rossi, S., Vignati, E.,GHG emissions of all world countries - 2021 Report, EUR 30831 EN, Publications Office of the European Union, Luxembourg, 2021, ISBN 978-92-76-41547-3, doi:10.2760/173513, JRC126363.

Granier, C., Darras, S., Denier van der Gon, H., Doubalova, J., Elguindi, N., Galle, B., Gauss, M., Guevara, M., Jalka- nen, J.-P., Kuenen, J., Liousse, C., Quack, B., Simpson, D., and Sindelarova, K.: The Copernicus Atmosphere Monitoring Service global and regional emissions (April 2019 version), Copernicus Atmosphere Monitoring Service (CAMS) report, https://doi.org/10.24380/d0bn-kx16, 2019.

Liu, Y., Qin, K., Cohen, B. J., Kang, H. S., Hu, W., Lu, F., Wu, X. H, Yang, C. L. : Analysis of the characteristics of methane in the coal mining area of southeastern Shanxi with eddy and mobile observation, Journal of China Coal Society, 47(12): 4395-4402, 2022.

MEE, 2019a. The People's Republic of China Second Biennial Update Report on Climate Change, Ministry of Ecology and Environment of People's Republic of China. available at: https://english.mee.gov.cn/Resources/Reports/reports/201907/P020190702568751604320.pdf (last access: August 9, 2023), 2019a.

MEE, 2019b. The People's Republic of China Third National Communication on Climate Change, Ministry of Ecology and Environment of People's Republic of China, available at: https://english.mee.gov.cn/Resources/Reports/reports/201907/P020190702566752327206.pdf (last access: August 9, 2023), 2019b.

National Bureau of Statistics of China. China Statistical Yearbook 2017. Ch. 9 (China Statistics Press, Beijing, China, 2017).

National Centers for Environmental Prediction/National Weather Service/NOAA/U.S. Department of Commerce: NCEP GDAS/FNL 0.25 Degree Global Tropospheric Analyses and Forecast Grids, Research Data Archive at the National Center for Atmospheric Research, Computational and Information Systems Laboratory, https://doi.org/10.5065/D65Q4T4Z (last access: 19 August 2023), 2015.

NDRC, 2017. The People's Republic of China First Biennial Update Report on Climate Change National Development and Reform Commission.

NDRC: The National Development and Reform Commission: The People's Republic of China Initial National Communications on Climate Change National (SNCCCC), Development and Reform Commission, available at: https://unfccc.int/sites/default/files/resource/China%20INC%20Chinese.pdf (last access: August 9, 2023), 2004.

NDRC: The National Development and Reform Commission: The People's Republic of China Second National Communication on Climate Change National (SNCCCC), Development and Reform Commission, available at: https://unfccc.int/resource/docs/natc/chnnc2e.pdf (last access: August 9, 2023), 2012.

SACMS, Compilation of National Coal Mine Methane Level Identification for 2011 (Beijing: China University of Mining and Technology Press), 2012.

UNFCCC, Greenhouse Gas Inventory Data Interface. https://di.unfccc.int/detailed_data_by_party. Last accessed 29 July 2023. 2021.

Butz, A., Guerlet, S., Hasekamp, O., Schepers, D., Galli, A., Aben, I., Frankenberg, C., Hartmann, J.-M., Tran, H., Kuze, A., Keppel-Aleks, G., Toon, G., Wunch, D., Wennberg, P., Deutscher, N., Griffith, D., Macatangay, R., Messerschmidt, J.,

https://doi.org/10.5194/egusphere-2023-2155
Preprint. Discussion started: 24 October 2023

Notholt, J., and Warneke, T.: Toward accurate CO2 and CH4 observations from GOSAT, Geophys. Res. Lett., 38, https://doi.org/10.1029/2011GL047888, 2011.

Etminan, M., Myhre, G., Highwood, E. J., and Shine, K. P.: Radiative forcing of carbon dioxide, methane, and nitrous oxide: A significant revision of the methane radiative forcing, Geophys. Res. Lett., 43, 12,614-12,623, https://doi.org/10.1002/2016GL071930, 2016.

Foy, B. de, Schauer, J. J., Lorente, A., and Borsdorff, T.: Investigating high methane emissions from urban areas detected by TROPOMI and their association with untreated wastewater, Environ. Res. Lett., 18, 044004, https://doi.org/10.1088/1748-9326/acc118, 2023.

Gao, J., Guan, C., and Zhang, B.: China's CH4 emissions from coal mining: A review of current bottom-up inventories, Sci. Total Environ., 725, 138295, https://doi.org/10.1016/j.scitotenv.2020.138295, 2020.

Gao, J., Guan, C., Zhang, B., and Li, K.: Decreasing methane emissions from China's coal mining with rebounded coal production, Environ. Res. Lett., 16, 124037, https://doi.org/10.1088/1748-9326/ac38d8, 2021.

de Gouw, J. A., Veefkind, J. P., Roosenbrand, E., Dix, B., Lin, J. C., Landgraf, J., and Levelt, P. F.: Daily Satellite Observations of Methane from Oil and Gas Production Regions in the United States, Sci. Rep., 10, 1379, https://doi.org/10.1038/s41598-020-57678-4, 2020.

Guerlet, S., Butz, A., Schepers, D., Basu, S., Hasekamp, O. P., Kuze, A., Yokota, T., Blavier, J.-F., Deutscher, N. M., Griffith, D. W. T., Hase, F., Kyro, E., Morino, I., Sherlock, V., Sussmann, R., Galli, A., and Aben, I.: Impact of aerosol and thin cirrus on retrieving and validating XCO2 from GOSAT shortwave infrared measurements, J. Geophys. Res. Atmospheres, 118, 4887–4905, https://doi.org/10.1002/jgrd.50332, 2013.

Hu, H., Landgraf, J., Detmers, R., Borsdorff, T., Aan de Brugh, J., Aben, I., Butz, A., and Hasekamp, O.: Toward Global Mapping of Methane With TROPOMI: First Results and Intersatellite Comparison to GOSAT, Geophys. Res. Lett., 45, 3682–3689, https://doi.org/10.1002/2018GL077259, 2018.

Janssens-Maenhout, G., Crippa, M., Guizzardi, D., Muntean, M., Schaaf, E., Dentener, F., Bergamaschi, P., Pagliari, V., Olivier, J. G. J., Peters, J. A. H. W., van Aardenne, J. A., Monni, S., Doering, U., Petrescu, A. M. R., Solazzo, E., and Oreggioni, G. D.: EDGAR v4.3.2 Global Atlas of the three major greenhouse gas emissions for the period 1970–2012, Earth Syst. Sci. Data, 11, 959–1002, https://doi.org/10.5194/essd-11-959-2019, 2019.

Li, M., Karu, E., Brenninkmeijer, C., Fischer, H., Lelieveld, J., and Williams, J.: Tropospheric OH and stratospheric OH and Cl concentrations determined from CH4, CH3Cl, and SF6 measurements, Npj Clim. Atmospheric Sci., 1, 1–7, https://doi.org/10.1038/s41612-018-0041-9, 2018.

Liu, G., Peng, S., Lin, X., Ciais, P., Li, X., Xi, Y., Lu, Z., Chang, J., Saunois, M., Wu, Y., Patra, P., Chandra, N., Zeng, H., and Piao, S.: Recent Slowdown of Anthropogenic Methane Emissions in China Driven by Stabilized Coal Production, Environ. Sci. Technol. Lett., 8, 739–746, https://doi.org/10.1021/acs.estlett.1c00463, 2021.

Lorente, A., Borsdorff, T., Butz, A., Hasekamp, O., aan de Brugh, J., Schneider, A., Wu, L., Hase, F., Kivi, R., Wunch, D., Pollard, D. F., Shiomi, K., Deutscher, N. M., Velazco, V. A., Roehl, C. M., Wennberg, P. O., Warneke, T., and Landgraf, J.: Methane retrieved from TROPOMI: improvement of the data product and validation of the first 2 years of measurements, Atmospheric Meas. Tech., 14, 665–684, https://doi.org/10.5194/amt-14-665-2021, 2021.

Pandey, S., Gautam, R., Houweling, S., van der Gon, H. D., Sadavarte, P., Borsdorff, T., Hasekamp, O., Landgraf, J., Tol, P., van Kempen, T., Hoogeveen, R., van Hees, R., Hamburg, S. P., Maasakkers, J. D., and Aben, I.: Satellite observations reveal

extreme methane leakage from a natural gas well blowout, Proc. Natl. Acad. Sci., 116, 26376–26381, https://doi.org/10.1073/pnas.1908712116, 2019.

Peng, S., Piao, S., Bousquet, P., Ciais, P., Li, B., Lin, X., Tao, S., Wang, Z., Zhang, Y., and Zhou, F.: Inventory of anthropogenic methane emissions in mainland China from 1980 to 2010, Atmospheric Chem. Phys., 16, 14545–14562, https://doi.org/10.5194/acp-16-14545-2016, 2016.

Plant, G., Kort, E. A., Murray, L. T., Maasakkers, J. D., and Aben, I.: Evaluating urban methane emissions from space using TROPOMI methane and carbon monoxide observations, Remote Sens. Environ., 268, 112756, https://doi.org/10.1016/j.rse.2021.112756, 2022.

Qin, K., Hu, W., He, Q., Lu, F., and Cohen, J. B.: Individual Coal Mine Methane Emissions Constrained by Eddy-Covariance Measurements: Low Bias and Missing Sources, EGUsphere, 1–49, https://doi.org/10.5194/egusphere-2023-1210, 2023.

Rigby, M., Montzka, S. A., Prinn, R. G., White, J. W. C., Young, D., O'Doherty, S., Lunt, M. F., Ganesan, A. L., Manning, A. J., Simmonds, P. G., Salameh, P. K., Harth, C. M., Mühle, J., Weiss, R. F., Fraser, P. J., Steele, L. P., Krummel, P. B., McCulloch, A., and Park, S.: Role of atmospheric oxidation in recent methane growth, Proc. Natl. Acad. Sci., 114, 5373–5377, https://doi.org/10.1073/pnas.1616426114, 2017.

Sadavarte, P., Pandey, S., Maasakkers, J. D., Lorente, A., Borsdorff, T., Denier van der Gon, H., Houweling, S., and Aben, I.: Methane Emissions from Superemitting Coal Mines in Australia Quantified Using TROPOMI Satellite Observations, Environ. Sci. Technol., 55, 16573–16580, https://doi.org/10.1021/acs.est.1c03976, 2021.

Saunois, M., Stavert, A. R., Poulter, B., Bousquet, P., Canadell, J. G., Jackson, R. B., Raymond, P. A., Dlugokencky, E. J., Houweling, S., Patra, P. K., Ciais, P., Arora, V. K., Bastviken, D., Bergamaschi, P., Blake, D. R., Brailsford, G., Bruhwiler, L., Carlson, K. M., Carrol, M., Castaldi, S., Chandra, N., Crevoisier, C., Crill, P. M., Covey, K., Curry, C. L., Etiope, G., Frankenberg, C., Gedney, N., Hegglin, M. I., Höglund-Isaksson, L., Hugelius, G., Ishizawa, M., Ito, A., Janssens-Maenhout, G., Jensen, K. M., Joos, F., Kleinen, T., Krummel, P. B., Langenfelds, R. L., Laruelle, G. G., Liu, L., Machida, T., Maksyutov, S., McDonald, K. C., McNorton, J., Miller, P. A., Melton, J. R., Morino, I., Müller, J., Murguia-Flores, F., Naik, V., Niwa, Y., Noce, S., O'Doherty, S., Parker, R. J., Peng, C., Peng, S., Peters, G. P., Prigent, C., Prinn, R., Ramonet, M., Regnier, P., Riley, W. J., Rosentreter, J. A., Segers, A., Simpson, I. J., Shi, H., Smith, S. J., Steele, L. P., Thornton, B. F., Tian, H., Tohjima, Y., Tubiello, F. N., Tsuruta, A., Viovy, N., Voulgarakis, A., Weber, T. S., van Weele, M., van der Werf, G. R., Weiss, R. F., Worthy, D., Wunch, D., Yin, Y., Yoshida, Y., Zhang, W., Zhang, Z., Zhao, Y., Zheng, B., Zhu, Q., Zhu, Q., and Zhuang, Q.: The Global Methane Budget 2000–2017, Earth Syst. Sci. Data, 12, 1561–1623, https://doi.org/10.5194/essd-12-1561-2020, 2020.

Scarpelli, T. R., Jacob, D. J., Maasakkers, J. D., Sulprizio, M. P., Sheng, J.-X., Rose, K., Romeo, L., Worden, J. R., and Janssens-Maenhout, G.: A global gridded (0.1° × 0.1°) inventory of methane emissions from oil, gas, and coal exploitation based on national reports to the United Nations Framework Convention on Climate Change, Earth Syst. Sci. Data, 12, 563–575, https://doi.org/10.5194/essd-12-563-2020, 2020.

Schneising, O., Buchwitz, M., Reuter, M., Vanselow, S., Bovensmann, H., and Burrows, J. P.: Remote sensing of methane leakage from natural gas and petroleum systems revisited, Atmospheric Chem. Phys., 20, 9169–9182, https://doi.org/10.5194/acp-20-9169-2020, 2020.

Sheng, J., Song, S., Zhang, Y., Prinn, R. G., and Janssens-Maenhout, G.: Bottom-Up Estimates of Coal Mine Methane Emissions in China: A Gridded Inventory, Emission Factors, and Trends, Environ. Sci. Technol. Lett., 6, 473–478, https://doi.org/10.1021/acs.estlett.9b00294, 2019.

https://doi.org/10.5194/egusphere-2023-2155
Preprint. Discussion started: 24 October 2023

Tu, Q., Hase, F., Schneider, M., García, O., Blumenstock, T., Borsdorff, T., Frey, M., Khosrawi, F., Lorente, A., Alberti, C., Bustos, J. J., Butz, A., Carreño, V., Cuevas, E., Curcoll, R., Diekmann, C. J., Dubravica, D., Ertl, B., Estruch, C., León-Luis, S. F., Marrero, C., Morgui, J.-A., Ramos, R., Scharun, C., Schneider, C., Sepúlveda, E., Toledano, C., and Torres, C.: Quantification of CH_4 emissions from waste disposal sites near the city of Madrid using ground- and space-based observations of COCCON, TROPOMI and IASI, Atmospheric Chem. Phys., 22, 295–317, https://doi.org/10.5194/acp-22-295-2022, 2022a.

Tu, Q., Schneider, M., Hase, F., Khosrawi, F., Ertl, B., Necki, J., Dubravica, D., Diekmann, C. J., Blumenstock, T., and Fang, D.: Quantifying CH_4 emissions in hard coal mines from TROPOMI and IASI observations using the wind-assigned anomaly method, Atmospheric Chem. Phys., 22, 9747–9765, https://doi.org/10.5194/acp-22-9747-2022, 2022b.

Varon, D. J., McKeever, J., Jervis, D., Maasakkers, J. D., Pandey, S., Houweling, S., Aben, I., Scarpelli, T., and Jacob, D. J.: Satellite Discovery of Anomalously Large Methane Point Sources From Oil/Gas Production, Geophys. Res. Lett., 46, 13507–13516, https://doi.org/10.1029/2019GL083798, 2019.

Veefkind, J. P., Aben, I., McMullan, K., Förster, H., de Vries, J., Otter, G., Claas, J., Eskes, H. J., de Haan, J. F., Kleipool, Q., van Weele, M., Hasekamp, O., Hoogeveen, R., Landgraf, J., Snel, R., Tol, P., Ingmann, P., Voors, R., Kruizinga, B., Vink, R., Visser, H., and Levelt, P. F.: TROPOMI on the ESA Sentinel-5 Precursor: A GMES mission for global observations of the atmospheric composition for climate, air quality and ozone layer applications, Remote Sens. Environ., 120, 70–83, https://doi.org/10.1016/j.rse.2011.09.027, 2012.

Zhang, Y., Gautam, R., Pandey, S., Omara, M., Maasakkers, J. D., Sadavarte, P., Lyon, D., Nesser, H., Sulprizio, M. P., Varon, D. J., Zhang, R., Houweling, S., Zavala-Araiza, D., Alvarez, R. A., Lorente, A., Hamburg, S. P., Aben, I., and Jacob, D. J.: Quantifying methane emissions from the largest oil-producing basin in the United States from space, Sci. Adv., https://doi.org/10.1126/sciadv.aaz5120, 2020.